Tricritical point and phase diagram based on critical scaling in monoaxial chiral helimagnet $Cr_{1/3}NbS_2$

Hui Han,[1,2] Lei Zhang,[1,*] Deepak Sapkota,[3] Ningning Hao,[1] Haifeng Du,[1] Min Ge,[4] Li Pi,[1,4] Changjin Zhang,[1] David G. Mandrus,[3,5,6,†] and Yuheng Zhang[1,4]

[1]*High Magnetic Field Laboratory, Chinese Academy of Sciences, Hefei 230031, China*
[2]*University of Science and Technology of China, Hefei 230026, China*
[3]*Department of Physics and Astronomy, The University of Tennessee, Knoxville, Tennessee 37996, USA*
[4]*Hefei National Laboratory for Physical Sciences at the Microscale, University of Science and Technology of China, Hefei 230026, China*
[5]*Materials Science and Technology Division, Oak Ridge National Laboratory, Oak Ridge, Tennessee 37831, USA*
[6]*Department of Materials Science and Engineering, The University of Tennessee, Knoxville, Tennessee 37996, USA*

(Dated: May 22, 2017)

The magnetism of the single crystal $Cr_{1/3}NbS_2$, which exhibits chiral soliton lattice (CSL) state, is investigated. The magnetization displays strong magnetic anisotropy when the field is applied perpendicularly and parallel to the c-axis in low field region ($H < H_S$, H_S is the saturation field). The critical exponents of $Cr_{1/3}NbS_2$ are obtained as $\beta = 0.370(4)$, $\gamma = 1.380(2)$, and $\delta = 4.853(6)$, which are close to the theoretical prediction of three-dimensional Heisenberg model. Based on the scaling equation and the critical exponents, the $H - T$ phase diagram in the vicinity of the phase transition is constructed, where two critical points are determined. One is a tricrtical point which locates at the intersection between the CSL, forced ferromagnetic (FFM), and paramagnetic (PM) states. The other one is a critical point situated at the boundaries between CSL, helimagnetic (HM), and PM states.

Magnetic materials with chirality have attracted considerable attention due to spin-textures such as helimagnetic (HM) structure, conical magnetic ordering, magnetic skyrmion, chiral bobber[1–5]. The chirality with spin-orbital coupling in the crystal structure results in an antisymmetric exchange interaction called the Dzyaloshinskii-Moriya (DM) interaction, which is 1∼2 orders of magnitude weaker than the ferromagnetic exchange interaction[6,7]. The competition between the DM interaction and the ferromagnetic exchange gives rise to the chiral spin-texture[8]. When an external magnetic field is applied above a threshold value, the HM ordering is usually modulated into exotic particle-like spin-texture such as skyrmion, magnetic soliton.

Recently, the monoaxial chiral magnets $Cr_{1/3}NbS_2$ becomes prominent due to the Chiral Magnetic Soliton Lattice (CSL), which is a type of superlattice structure consist of periodic helical spin texture[9–11]. The crystal structure for $Cr_{1/3}NbS_2$ belongs to the space group $P6_322$[12,13]. The hexagonal layers in 2H-NbS_2 are intercalated by the Cr ions which are in the trivalent state with localized moments $S = 3/2$, whereas the electronic conduction originates from an unfilled band of Nb atoms. Due to the strong magnetocrystalline anisotropy and DM interaction, $Cr_{1/3}NbS_2$ displays a ground state of helical magnetic ordering with vector along the c-axis[13,14]. The magnetic sate can be modulated differently through the direction of the applied field H. When H is applied parallel to the c-axis, the HM ordering is polarized to conical ordering, and finally to forced ferromagnetical (FFM) phase. However, when H is applied perpendicularly to the c-axis, the HM structure with 48 nm is modulated continuously into a CSL state, which is well reproduced by the one-dimensional chiral sine-Gordon model[10]. Further increase of H results in a phase transition from an incommensurate CSL to a commensurate FFM state[15]. It has been demonstrated that CSL can be effectively manipulated by the magnetic field or current injection, which implies potential application as spintronic device[16–18].

Although the phase transition and CSL in $Cr_{1/3}NbS_2$ have been investigated intensively, controversies emerge for the complex phase diagrams[19–23]. The phase diagrams have been constructed by several experimental and theoretical works[12,15,24–27]. However, open contradiction exists on boundaries between different phases, especially in the vicinity of the phase transition, which seriously hinders the understanding of the physical properties in $Cr_{1/3}NbS_2$. In this work, the magnetism of the single crystal $Cr_{1/3}NbS_2$ is investigated, which displays strong magnetic anisotropy. Moreover, the critical behavior unambiguously suggests that the magnetic coupling is of a three-dimensional (3D) Heisenberg type. Based on the critical exponents and scaling equation, the $H - T$ phase diagram is clearly constructed, where two critical points are determined.

The physical properties of single crystal $Cr_{1/3}NbS_2$ are described in the supplementary material[28]. Figure 1 (a) and (b) gives the temperature dependence of magnetization $[M(T)]$ under selected field, where the external field is applied perpendicularly and parallel to the c-axis respectively. All $M(T)$ curves with $H \perp c$ or $H//c$ undergo a magnetic ordering transition at the phase transition temperature $T_C \sim 125$ K, which is in agreement with previous report[13]. However, the $M(T)$ curves exhibit very different behaviors when $H \perp c$ and $H//c$. When

$H \perp c$, $M(T)$ curves below $H = 500$ Oe almost display the same behavior, as shown in Fig. 1 (a). However, when H exceeds 500 Oe, the values under fixed field increases abruptly. On the other hand, when $H//c$, $M(T)$ curves is raised monotonously with the applied field. As indicated by the $M(T)$ curves, the monoaxial $Cr_{1/3}NbS_2$ exhibits strong anisotropic magnetization, which should be investigated by the angle dependent of magnetization $[M(\varphi)]$. Figure 1 (c) and (d) shows the out-of-plane and in-plane $M(\varphi)$ at 2 K. The in-plane $M(\varphi)$ was measured under the field within the ab-plane, while the out-of-plane one was performed under the field rotated from ab-plane to c-axis[28]. It can be seen from Fig. 1 (c) that the out-of-plane $M(\varphi)$ at 2 K exhibits a shape of butterfly, which suggests very strong magnetic anisotropy. However, the in-plane $M(\varphi)$ display isotropic magnetization, as shown in Fig. 1 (d). The magnetization in ab-plane is much strong than that along c-axis, suggesting that the spins are ordered within the ab-plane.

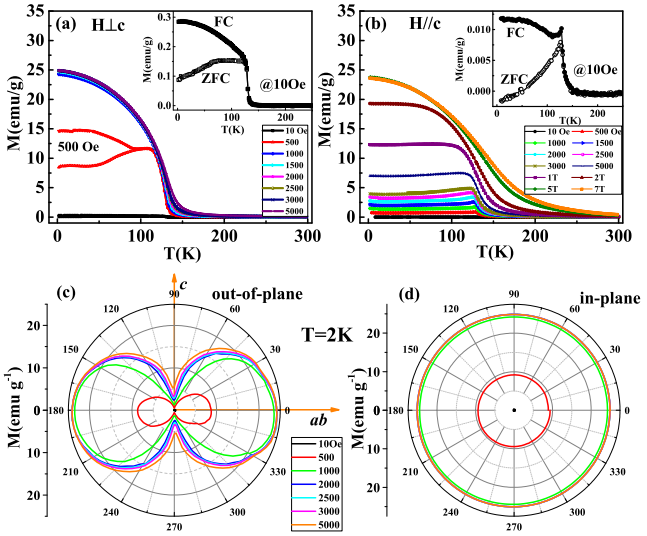

FIG. 1: Temperature dependence of magnetization $[M(T)]$ under selected fields for $Cr_{1/3}NbS_2$ with (a) $H \perp c$ and (b) $H//c$; magnetization as a function of rotation angel $[M(\varphi)]$ at 2 K for (c) the out-of-plane and in-plane one.

Figure 2 (a) plot the isothermal magnetization $[M(H)]$ at selected temperature with $H \perp c$. For $M(H)$ with $H \perp c$ at 2 K and 100 K below T_C, two symmetrical magnetic steps appear in low field region before saturation. Moreover, a loop is found at the magnetic step between increase and decrease of field, which has been also found in previous works[29]. However, when $H//c$, no step or loop is found on the $M(H)$ curves[28]. The loop becomes smaller when temperature increases, which disappears when temperature exceeds 120 K, as shown in Fig. 2 (b). It is well known that $Cr_{1/3}NbS_2$ undergoes a field-induced transition from HM to CSL below T_C. Moreover, the CSL state is polarized to FFM, accompanied with

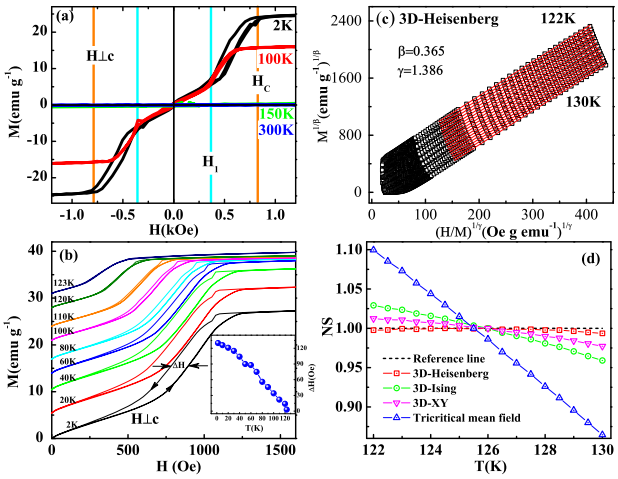

FIG. 2: (a) Isothermal magnetization as a function of field $[M(H)]$ at selected temperature with $H \perp c$; (b) $M(H)$ loops $[\Delta H]$ when $H \perp c$ [the curves are elevated vertically for clarity, the inset shows ΔH as a function of temperature]; (c) the modified Arrott plot based on the 3D-Heisenberg model; (d) temperature dependence of normalized slope (NS) for the four theoretical models.

a transition from incommensurate to commensurate states. The $M(H)$ loops are similar to those observed in the metastable ferrimagnetic or antiferromagnetic state, where $M(H)$ loop occurs between phase transitions induced by the field[30]. Thus, $M(H)$ loops in $Cr_{1/3}NbS_2$ suggests that the CSL is a metastable state.

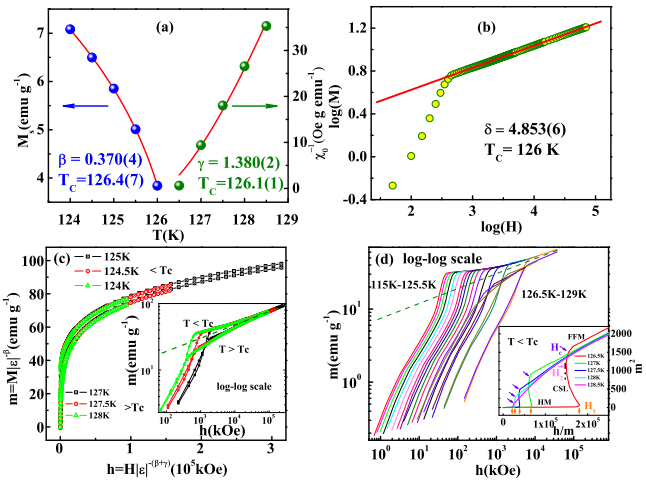

FIG. 3: (a) The M_S (left) and $\chi_0{}^{-1}$ (right) as a function of temperature for $Cr_{1/3}NbS_2$; (b) isothermal $M(H)$ at T_C on log-log scale (all red solid curves are fitted); (c) scaling plot of m vs. h around T_C (the inset shows typical $m(h)$ on log-log scale); (d) the magnification of m vs. h in low field region (the inset shows the re-scaling of m^2 vs. h/m).

In order to uncover the magnetic coupling in

$Cr_{1/3}NbS_2$, the critical behavior should be investigated. Figure S5 (a) gives the initial isothermal $M(H)$ around T_C with $H \perp c$, and the Arrott plot of M^2 vs. H/M is depicted in Fig. S5 (b)[28]. All curves on the Arrott plot display nonlinear behaviors even in the high field region, which suggests that the magnetic interaction in $Cr_{1/3}NbS_2$ cannot be described by the conventional Landau mean-field model[31,32]. The order of the phase transition can be determined by the slope from the Arrott plot according to the Banerjee's criterion, where a negative slope suggests first-order transition and a positive slope implies a second-order one[33]. The positive slopes of M^2 vs. H/M curves reveal that the phase transition in $Cr_{1/3}NbS_2$ is of a second order.

In view of the conventional Arrott pot is invalid for $Cr_{1/3}NbS_2$, the modified Arrott plot based on the critical exponents should be constructed. As we know, in the vicinity of a second order magnetic phase transition, the spontaneous magnetization M_S and initial susceptibility χ_0 can be described by a series of functions[34,35]:

$$M_S(T) = M_0(-\varepsilon)^{\beta}, \varepsilon < 0, T < T_C \tag{1}$$

$$\chi_0^{-1}(T) = (h_0/M_0)\varepsilon^{\gamma}, \varepsilon > 0, T > T_C \tag{2}$$

$$M = DH^{1/\delta}, \varepsilon = 0, T = T_C \tag{3}$$

where $\varepsilon = (T - T_C)/T_C$ is the reduced temperature; M_0/h_0 and D are critical amplitudes. The parameters β (associated with M_S), γ (associated with χ_0), and δ (associated with T_C) are the critical exponents. The critical behavior around the critical temperature can be revealed by the critical exponents, which follow the Arrott-Noakes equation of state in asymptotic critical region[36]:

$$(H/M)^{1/\gamma} = (T - T_C)/T_C + (M/M_1)^{1/\beta} \tag{4}$$

The critical exponents gives significant clues of magnetic interactions, such as the correlating length, spin-dimensionality, and decaying distance of magnetic coupling. Four series of critical exponents belonging to the 3D-Heisenberg model ($\beta = 0.365$, $\gamma = 1.386$), 3D-Ising model ($\beta = 0.325$, $\gamma = 1.24$), 3D-XY model ($\beta = 0.345$, $\gamma = 1.316$), and tricritical mean-field model ($\beta = 0.25$, $\gamma = 1.0$) are tried to construct the modified Arrott plots[32,37], as shown in Fig. 2 (c) (others are shown in Fig. S6 in the supplementary material[28]). All the curves in these four constructions exhibit quasi-straight lines in high field region. For an ideal model, the modified Arrott plot should display a series of parallel lines in high field region with the same slope, where the slope is defined as $S(T) = dM^{1/\beta}/d(H/M)^{1/\gamma}$. The normalized slope ($NS$) is defined as $NS = S(T)/S(T_C)$, which enables us to distinguish the most suitable model by comparing the NS with the ideal value of '1'[38–40]. Plot of NS vs. T for the four different models is shown in Fig. 2 (d). It can be seen that the NS of 3D-Heisenberg model is close to '1' mostly among these models, which indicates that the critical behavior of $Cr_{1/3}NbS_2$ is mostly close to the 3D-Heisenberg model.

The critical exponents β and γ can be obtained by the iteration method[41]. The linear extrapolation from high field region to the intercepts with the axes of $M^{1/\beta}$ and $(H/M)^{1/\gamma}$ yields $M_S(T,0)$ and $\chi_0^{-1}(T,0)$. By fitting to Eqs. (1) and (2), a set of β and γ is obtained, which are used to reconstruct a new modified Arrott plot. Subsequently, new $M_S(T,0)$ and $\chi_0^{-1}(T,0)$ are generated from the linear extrapolation from high field region. By this way, another set of β and γ can be obtained. This procedure is repeated until β and γ hardly change. The obtained critical exponents by the iteration method are independent on the initial parameters. In this way, $\beta = 0.370(4)$ with $T_C = 126.4(7)$ and $\gamma = 1.380(2)$ with $T_C = 126.1(1)$ are obtained for $Cr_{1/3}NbS_2$, as shown in Fig 3 (a). The obtained T_C is consistent with that obtained by T. Miyadai *et al*[13]. Figure 3 (b) shows the initial $M(H)$ at the critical temperature $T_C = 126$ K, with the inset plotted on a $\log - \log$ scale. One can see that the $M(H)$ at T_C exhibits a straight line on a $\log - \log$ scale when $H > H_S$. Thus, $\delta = 4.853(6)$ is determined in the high field region ($H > H_S$) based on Eq. (3). According to the statistical theory, these critical exponents should fulfill the Widom scaling law[42]:

$$\delta = 1 + \frac{\gamma}{\beta} \tag{5}$$

According to the Widom scaling law $\delta = 4.729(7)$ is calculated, which in agreement with that obtained from the experimental critical isothermal analysis. The self-consistency of the critical exponents demonstrates that they are reliable and confirmatory.

The experimentally obtained critical exponents ($\beta = 0.370(4)$, $\gamma = 1.380(2)$, $\delta = 4.853(6)$) are very close to the theoretical prediction of 3D-Heisenberg model ($\beta = 0.365$, $\gamma = 1.386$, $\delta = 4.80$)[32], which suggests a short-rang magnetic coupling of Cr-Cr. Moreover, it can be calculated that $\sigma = 1.932(6)$ for $Cr_{1/3}NbS_2$[41], which indicates that the magnetic interaction decays on spatial distance as $J(r) \sim r^{-4.9}$. Subsequently, it gives the correlation length critical exponent $\nu = 0.714(2)$ with $\xi = \xi_0|T - T_C|^{-\nu}$ (where ξ is the correlation length, and $\nu = \gamma/\sigma$). As we know, these critical exponents should follow the scaling equations. Defining the renormalized magnetization $m \equiv \varepsilon^{-\beta}M(H,\varepsilon)$ and the renormalized field $h \equiv H\varepsilon^{-(\beta+\gamma)}$, in the asymptotic critical region the scaling equations can be written as[34]:

$$m = f_{\pm}(h) \tag{6}$$

where $f_{\pm}$ are regular functions denoted as f_+ for $T > T_C$ and f_- for $T < T_C$. The scaling equations indicate that m vs. h should form two universal branches for $T > T_C$ and $T < T_C$ respectively, even those in low field region[43,44]. However, if a field-induced phase transition occurs, the scaling will become divergent at the boundaries between the different phases. The divergence of

the scaling curves supplies an effective method to distinguish the different phases, especially those vague phase boundaries[41]. Based on the scaling equation, the initial $M(H)$ curves around T_C for $Cr_{1/3}NbS_2$ are replotted as $m(h)$ in Fig. 3 (c), with several typical curves on log-log scale in the inset. It can be seen that experimental $M-H$ curves collapse into two universal branches, except those in the low field region. Especially, all m vs. h curves on log-log scale are depicted in Fig. 3 (d), with the re-scaling plot of m^2 vs. h/m in the inset. The m^2 vs. h/m curves clearly display the magnetic transitions in low field region, as shown in the inset of Fig. 3 (d). Three regions separated by two magnetic transitions are clearly observed from the m^2 vs. h/m curves, which are corresponding to the HM, CSL, and FFM states respectively. In very low field region, a plateform is found on m^2 vs. h/m curves, which is corresponding to the HM state. With the increase of field to H_1, an abrupt increase occurs to m^2 vs. h/m. Considering the partial polarization of moments from HM to CSL, this abrupt increase of m^2 vs. h/m is attributed to the CSL transition. When H exceeds H_C, the CSL is completely polarized into FFM state. In the CSL region, the state can be further distinguished by the slop (S) of m^2 vs. h/m. The region of $S<0$ is corresponding to CSL1 (dominant helical texture with poor FM array), and that for $S>0$ corresponding to CLS2 (with large FM array)[15]. In fact, the region of CLS2 with $S<0$ has approached the FFM phase whose S is also negative on the m^2 vs. h/m curve.

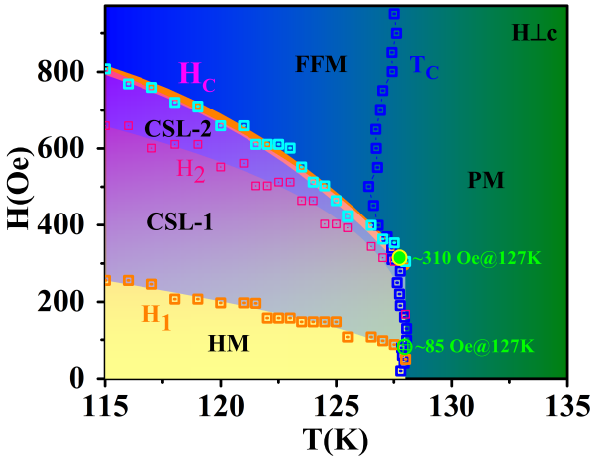

FIG. 4: The $H-T$ phase diagram in the vicinity of the phase transition for $Cr_{1/3}NbS_2$ obtained by the scaling of m^2 vs. h/m.

Based on the scaling curves of the m^2 vs. h/m, the $H-T$ phase diagram with $H\perp c$ is constructed in Fig. 4. It can be seen that $Cr_{1/3}NbS_2$ exhibits a HM ground state below $T_C\sim 127$ K. When the field is applied, the HM state persists below H_1. When H exceeds H_1, the HM state is modulated to CSL1. Subsequently, CSL1 is changed to CSL2 state when $H>H_2$. Finally, the CSL2 state is polarized into FFM phase when H exceeds H_C. Two critical points can be determined on the $H-T$ phase diagram, as shown in Fig. 4. In fact, in the monoaxial chiral helimagnetic system, two tricritical points have been predicted theoretically by V. Laliena *et al.* when the field is applied along variable directions[27]. In addition, in another work, they suggests a tricritical point and a zero-field critical one in monoanixal helimagnet when field is applied along the c-axis[24]. The zero-field critical point locates at boundary from HM to PM phases[24]. Therefore, in present case, one critical point corresponds to a tricrtical one, which locates at the intersection between the CSL, FFM, and PM phases ($\sim$ 310 Oe at 127 K). The other one is determined as zero-field critical point, which is situated at the boundaries between HM, CSL and PM phases ($\sim$ 85 Oe at 127 K).

In summary, the magnetism of the single crystal $Cr_{1/3}NbS_2$ is investigated. The magnetization displays strong magnetic anisotropy when the external field is applied parallel and perpendicularly to the c-axis. The $M(H)$ curve with $H\perp c$ displays a loop on the boundary of the phase transition from incommensurate CSL to commensurate FFM, which suggests that the CSL phase is a metastable state. The critical exponents of $Cr_{1/3}NbS_2$ are obtained as $\beta=0.370(4)$, $\gamma=1.380(2)$, and $\delta=4.853(6)$, which is close to the theoretical prediction of 3D-Heisenberg model. The critical behavior indicates the magnetic coupling is of a short-range type. Based on the scaling equation, the $H-T$ phase diagram around T_C is constructed, where two critical points are determined. One critical point is a tricritical one, which locates at the intersection between the CSL, FFM, and PM states. The other critical point is a zero-field critical one, which is situated at the intersection between CSL, HM and PM states.

This work was supported by the National Natural Science Foundation of China (Grant Nos. 11574322, 11474290, and 11574288). D. S. and D. G. M. acknowledge support from the National Science Foundation under grant DMR-1410428.

* Corresponding author. Email:zhanglei@hmfl.ac.cn
† Corresponding author. Email:dmandrus@utk.edu

[1] U. K. Roβler, A. N. Bogdanov, C. Pfleiderer, Nature (London) **442,** 797 (2006).
[2] S. Muuhlbauer *et al.*, Science **323,** 915 (2009).
[3] X. Yu *et al.*, Nature (London) **465,** 901 (2010).

[4] S. Seki, X. Z. Yu, S. Ishiwata, and Y. Tokura, Science, **336,** 198 (2012).
[5] F. N. Rybakov, A. B. Borisov, S. Blugel, and N. S. Kiselev, Phys. Rev. Lett. **115,** 117201 (2015).
[6] I. Dzyaloshinsky, J. Phys. Chem. Solids **4,** 241 (1958).
[7] T. Moriya, Phys. Rev. **120,** 91 (1960).
[8] A. Bauer and C. Pfleiderer, Phys. Rev. B **85,** 214418 (2012).
[9] Y. Togawa *et al.*, Phys. Rev. Lett. **111,** 197204 (2013).
[10] Y. Togawa *et al.*, Phys. Rev. Lett. **108,** 107202 (2012).
[11] Y. Masaki and R. L. Stamps,Phys. Rev. B **95,** 024418 (2017).
[12] N. J. Ghimire *et al.*, Phys. Rev. B **87,** 104403 (2013).
[13] T. Miyadai *et al.*, J. Phys. Soc. Jpn. **52,** 1394 (1983).
[14] F. Hulliger and E. Pobitschka, J. Solid State Chem. **1,** 117 (1970).
[15] K. Tsuruta *et al.*, Phys. Rev. B **93,** 104402 (2016).
[16] J. Kishine, A. S. Ovchinnikov, and I. V. Proskurin, Phys. Rev. B **82,** 064407 (2010).
[17] A. B. Borisov, J. Kishine, I. G. Bostrem, and A. S. Ovchinnikov, Phys. Rev. B **79,** 134436 (2009).
[18] K. Koumpouras, A. Bergman, O. Eriksson, D. Yudin, Sci. Rep. **6,** 25685 (2016).
[19] S. Mankovsky, S. Polesya, H. Ebert, W. Bensch, Phys. Rev. B **94,** 184430 (2016).
[20] N. Sirica *et al.*, Phys. Rev. B **94,** 075141 (2016).
[21] Y. Togawa, Y. Kousaka, K. Inoue, and J. Kishine, J. Phys. Soc. Jpn. **85,** 112001 (2016).
[22] Y. Togawa *et al.*, Phys. Rev. B **92,** 220412(R) (2015).
[23] B. Chapman, A. Bornstein, N. Ghimire, D. Mandrus, and M. Lee, Appl. Phys. Lett. **105,** 072405 (2014).
[24] V. Laliena, J. Campo, Y. Kousaka, Phys. Rev. B **94,** 094439 (2016).
[25] Y. Nishikawa and K. Hukushima, Phys. Rev. B **94,** 064428 (2016).
[26] M. Shinozaki, S. Hoshino, Y. Masaki, J. Kishine, and Y. Kato, J. Phys. Soc. Jpn. **85,** 074710 (2016).
[27] V. Laliena *et al.*, Phys. Rev. B **93,** 134424 (2016).
[28] Please see the online Supplementary Material.
[29] K. Tsuruta *et al.*, J. Phys. Soc. Jpn **85,** 013707 (2016).
[30] E. Stryjewski and N. Giordano, Adv. Phys. **26,** 487 (1977).
[31] A. Arrott, Phys. Rev. **108,** 1394 (1957).
[32] S. N. Kaul, J. Magn. Magn. Mater. **53,** 5 (1985).
[33] S. K. Banerjee, Phys. Lett. **12,** 16(1964).
[34] H. E. Stanley, *Introduction to Phase Transitions and Critical Phenomena* (Oxford University Press, London, 1971).
[35] M. E. Fisher, Rev. Mod. Phys. **46,** 597 (1974).
[36] A. Arrott and J. Noakes, Phys. Rev. Lett. **19,** 786 (1967).
[37] K. Huang, *Statistical Mechanics*, 2nd ed. (Wiley, New York, 1987).
[38] L. Zhang *et al.*, Phys. Rev. B **85,** 104419 (2012).
[39] J. Y. Fan *et al.*, Phys. Rev. B **81,** 144426 (2010).
[40] L. Zhang *et al.*, Europhys. Lett. **91,** 57001 (2010).
[41] L. Zhang, *et al.*, Phys. Rev. B **91,** 024403 (2015).
[42] L. P. Kadanoff, Physics **2,** 263 (1966).
[43] M. H. Phan *et al.*, J. Alloys Compd. **508,** 238 (2010).
[44] N. Khan *et al.*, Phys. Rev. B **82,** 064422 (2010).